JGR Solid Earth

RESEARCH ARTICLE
10.1029/2018JB016415

Special Section:
Physical Properties of Rocks, Friction and Fracturing: The Walsh Volume

The Effect of Water on Fe-Mg Interdiffusion Rates in Ringwoodite and Implications for the Electrical Conductivity in the Mantle Transition Zone

Baohua Zhang[1], **Takashi Yoshino**[2], **and Chengcheng Zhao**[2]

[1]Key Laboratory for High-Temperature and High-Pressure Study of the Earth's Interior, Institute of Geochemistry, Chinese Academy of Sciences, Guiyang, China, [2]Institute for Planetary Materials, Okayama University, Tottori, Japan

Abstract We determined the kinetics of Fe-Mg interdiffusion in ringwoodite aggregates as a function of water content (up to ~6,000 wt. ppm H_2O) at 20 GPa and 1,373–1,673 K by the diffusion couple method. The dependence of Fe-Mg interdiffusivity ($D_{Fe\text{-}Mg}$) on Fe concentration was determined using the Boltzmann-Matano method. The experimentally reported $D_{Fe\text{-}Mg}$ in ringwoodite within $0 \le X_{Fe} \le 0.1$ could be fitted by the relation $D_{Fe\text{-}Mg}(m^2/s) = D_0 X_{Fe}^n C_{H_2O}^r \exp\left[-\left(E^* + \alpha C_{H_2O}\right)/RT\right]$, where $E^* = (1 - X_{Fe})E_{Mg} + X_{Fe}E_{Fe}$ ($E_{Mg} = 140 \pm 5$ kJ/mol, $E_{Fe} = 4 \pm 2$ kJ/mol), $D_0 = 5.59^{+2.90}_{-1.91} \times 10^{-10}$ m^2/s, $n = -0.21 \pm 0.10$, $r = 0.25 \pm 0.03$, and $\alpha = -24 \pm 4$. The water content exponent r of 0.25 suggests a nonnegligible role of water in enhancing Fe-Mg interdiffusion in ringwoodite. The length scale over which the chemical heterogeneities are homogenized by Fe-Mg interdiffusion in the mantle transition zone is estimated to be only a few hundred meters even assuming the whole Earth age. Comparison between the conductivities predicted from Fe-Mg interdiffusion and those obtained from magnetotelluric surveys suggests that around 0.1 wt.% water can account for the high conductivity anomalies (~$10^{-0.6}$–10^{-1} S/m) observed in the lower part of the mantle transition zone.

Key Points:
- Effect of water on $D_{Fe\text{-}Mg}$ in ringwoodite was investigated under 20 GPa
- The length scales for homogenization of chemical heterogeneity in the MTZ are limited
- The 0.1 wt.% H_2O can account for high conductivity anomalies observed in the lower part of the MTZ

Supporting Information:
- Supporting Information S1
- Data Set S1

Correspondence to:
B. Zhang,
zhangbaohua@vip.gyig.ac.cn

Citation:
Zhang, B., Yoshino, T., & Zhao, C. (2019). The effect of water on Fe-Mg interdiffusion rates in ringwoodite and implications for the electrical conductivity in the mantle transition zone. *Journal of Geophysical Research: Solid Earth*, *124*, 2510–2524. https://doi.org/10.1029/2018JB016415

Received 28 JUL 2018
Accepted 29 JAN 2019
Accepted article online 2 FEB 2019
Published online 14 MAR 2019
Corrected 25 MAR 2019

This article was corrected on 25 MAR 2019. See the end of the full text for details.

1. Introduction

Ringwoodite [γ-$(Mg,Fe)_2SiO_4$] is the major component of the lower mantle transition zone (MTZ), which can contain significant amount of water in its crystal structure (Kohlstedt et al., 1996). Therefore, the MTZ is considered to be a large water reservoir in deep Earth (Inoue et al., 1995; Ohtani et al., 2004). It has been demonstrated that the incorporation of even tens of parts per million water by weight (wt. ppm) water could significantly affect physical properties of ringwoodite including seismic wave velocity (Jacobsen et al., 2004) and electrical conductivity (Huang et al., 2005; Yoshino et al., 2008).

Atomic diffusion in ringwoodite is the rate-limiting process influencing chemical mixing and equilibration, mass, and charge transports. Although diffusivities of Fe-Mg, Si, and O were measured in a number of studies (e.g., Farber et al., 1994, 2000; Shimojuku et al., 2009), none of the studies considered the effect of water. It was revealed that olivine and wadsleyite (low-pressure polymorphs of ringwoodite) exhibited high dependence of diffusivity on water content (e.g., Hier-Majumder et al., 2005; Kubo et al., 2004). Therefore, the probable importance of water on the atomic diffusion in ringwoodite should not be neglected to understand and further constrain geodynamic processes in the MTZ (Chakraborty, 2008; Watson & Baxter, 2007).

Among various atoms in ringwoodite, Fe-Mg is the fastest diffusing species, providing the upper limit of related processes, and the effect of water on its $D_{Fe\text{-}Mg}$ might be larger than that in olivine (Hier-Majumder et al., 2005). To verify this speculation, we determined the water effect on $D_{Fe\text{-}Mg}$ of synthetic Fe-free (Mg_2SiO_4) and Fe-bearing ($Fe_{0.2}Mg_{1.8}SiO_4$) ringwoodite aggregates under high temperature and high pressure in this study. The role of water in homogenization of chemical heterogeneities in the MTZ was discussed, and the possible MTZ water storage was estimated by means of the inferred conductivity of ringwoodite from present $D_{Fe\text{-}Mg}$ data.

2. Experimental Methods and Analyses

2.1. Synthesis of Ringwoodite Aggregates

Fe-free (Mg_2SiO_4) and Fe-bearing ($Fe_{0.2}Mg_{1.8}SiO_4$) ringwoodite aggregates were synthesized from forsterite and natural San Carlos olivine powder, respectively, at 20 GPa and 1,473–1,723 K using the Kawai-type

Table 1
Summary of Experimental Conditions and Results of Fe-Mg Interdiffusion Coefficients in Ringwoodite

Run	T (K)	Time (hr)	Diffusion couple	C_{H2O} [a] (wt. ppm)	C_{H2O} [b] (wt. ppm)	$D_{Fe\text{-}Mg}$ (m^2/s) for X_{Mg} = 0.94 [c]	$D_{Fe\text{-}Mg}$ (m^2/s) for X_{Mg} = 0.96 [d]	Capsule	d (μm) [e]	d (μm) [f]
1K2773	1,373	37	Nominally dry	39(23)/40(18) [g]	40(12)/74(17)	$2.99\ (0.13) \times 10^{-15}$	$2.70\ (0.09) \times 10^{-15}$	MgO + Fe	70/6	82/8
1K2762	1,523	46	Nominally dry	70(15)/80(24)	74(9)/92(14)	$6.31\ (0.16) \times 10^{-15}$	$5.39\ (0.12) \times 10^{-15}$	MgO + Fe	25/20	30/25
1K2772	1,573	20	Nominally dry	39(23)/40(18)	55(11)/ 56(21)	$7.95\ (0.13) \times 10^{-15}$	$7.03\ (0.06) \times 10^{-15}$	MgO + Fe	10/6	13/8
5K3105	1,673	30	Nominally dry	70(15)/80(24)	n.d. [h]/73(15)	$2.27\ (0.08) \times 10^{-14}$	$2.07\ (0.14) \times 10^{-14}$	MgO + Fe	18/15	25/20
1K2766	1,573	36	Wet	3,000(120)/3,087(188)	2,895(75)/2,914(102)	$6.61\ (0.12) \times 10^{-14}$	$5.12\ (0.13) \times 10^{-14}$	Pt	70/45	100/60
1K2773	1,373	37	Wet	6,032(215)/6,265(149)	4,705(88)/ 4,961(132)	$1.82\ (0.18) \times 10^{-14}$	$1.59\ (0.21) \times 10^{-14}$	Pt	40/20	55/25
1K2772	1,573	20	Wet	6,032(215)/6,265(149)	n.d./514(73).	$2.05\ (0.26) \times 10^{-14}$	$1.76\ (0.25) \times 10^{-14}$	Pt	40/20	65/35

Note. All experiments were performed under 20 GPa.
[a]Water content before diffusion annealing measured by Fourier transform infrared. [b]Water content after diffusion annealing measured by Fourier transform infrared. [c]The average of $D_{Fe\text{-}Mg}$ between X_{Mg} = 0.93 and X_{Mg} = 0.95. The range of uncertainties is given in parentheses. [d]The average of $D_{Fe\text{-}Mg}$ between X_{Mg} = 0.95 and X_{Mg} = 0.97. The range of uncertainties is given in parentheses. [e]Grain size before diffusion experiment. [f]Grain size after diffusion experiment. [g]The values before and after forward slash in each run indicate the water content/or grain size obtained from Mg-rich side and Fe-rich side to the diffusion interface, respectively. The range of uncertainties is given in parentheses. [h]n.d. means the water content was not determined due to the lost sample or the absence of clear infrared absorption peaks.

multianvil press. The starting forsterite is prepared from synthetic forsterite single crystal (Oxide Company) grown parallel to *b* axis by the Czochralski technique whose chemical composition was reported by Fei et al. (2012). For dry condition experiments, forsterite or olivine powder was placed in Fe foil capsule, which can effectively remove water from the sample (Irifune et al., 2016) while at the same time maintaining fO_2 close to the Fe-FeO (IW) buffer condition. The truncated edge length of the second-stage tungsten carbide anvil is 5 mm. The pressure assembly consists of 10-mm Cr_2O_3-doped MgO octahedron, a ZrO_2 thermal insulation sleeve, a $LaCrO_3$ cylindrical heater, and a MgO sleeve which insulates the metal capsule from the furnace (see supporting information Figure S1). The cell assembly was compressed to 20 GPa and then heated to 1,573 and 1,623 K for dry and hydrous samples, respectively, with temperature measured by a $W_{97}Re_3$-$W_{75}Re_{25}$ thermocouple. After annealing at target temperature for 30 min until forsterite or olivine transformed to ringwoodite, the power supply was switched off, and pressure was released slowly. In the recovered samples, only ringwoodite phase was identified by X-ray micro-diffractometer (Rigaku RAPID II; see Figure S2). Hydrous ringwoodite aggregates (both iron-free and iron-bearing) were obtained following the same method as described above but with olivine or forsterite powder welded in a Pt capsule together with powder mixtures of talc + brucite (1.4:1 in wt.%) served as water source. The oxygen fugacity of olivine in Pt capsule is about two orders of magnitude higher than that in Fe capsule (Faul et al., 2018). Average grain size (*d*; Table 1) was analyzed using the intercept method on corresponding secondary electron microscope images (JEOL JXL8800M) and estimated from the measured average intercept length (*L*) using the relationship $d = cL$, where c is a constant value of 1.56 (Mendelson, 1969). The variation of intercept length was determined from the measured length between two intercepts (i.e., grain boundary) along analyzed lines.

2.2. $D_{Mg\text{-}Fe}$ Interdiffusion Experiment

Disks with ~0.4-mm-thick and ~1-mm diameter were cored from sliced pieces for both dry and hydrous synthetic ringwoodite aggregates by ultrasonic drilling machine. One surface of these disks was polished with 0.25 μm diamond powder and then closely contacted with each other for subsequent interdiffusion experiments. For nominally dry experiments, a pair of Fe-free and Fe-bearing ringwoodite synthesized under dry conditions was assembled as a diffusion couple and inserted into a Fe capsule (Figure 1a). Hydrous diffusion pairs synthesized under hydrous condition consisted of Fe-free and Fe-bearing ringwoodite aggregates with similar water content and were welded in a Pt capsule. Afterward, the dry and hydrous diffusion couples were annealed at 20 GPa and 1,373–1,673 K for 20–46 hr (Table 1) using the same cell assembly as that for synthesis experiment. As shown in Figure 1b, in some experiments, two diffusion couples (both water-doped and water-undoped ones) were placed in the same run (e.g., 1K2772 and 1K2773). The sample was first pressurized to 20 GPa and then heated to target temperature, which was controlled within ±5 K during annealing.

2.3. FTIR analysis

Prior to the diffusion experiment, one piece of ringwoodite aggregate was double polished to ~70 μm and ~150 μm thickness for hydrous and anhydrous one, respectively, for Fourier transform infrared (FTIR) measurement. The section was heated at ~473 K in a vacuum oven for 24 hr to remove surface absorbed water. The unpolarized FTIR spectra were obtained from crack-free areas with 40 × 40 μm^2 aperture size on sample surface using Jasco FTIR-6200 Equipper

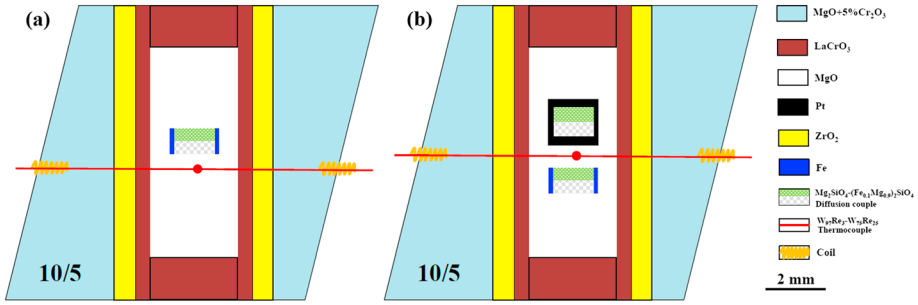

Figure 1. Schematic drawing of cell assemblies for high pressure diffusion experiments. Assemblies (a) and (b) were adopted in the experiments with dry diffusion couples and two diffusion couples (dry and wet) at 20 GPa, respectively.

with IRT-7000 infrared microscope. At least five different spots were measured for each sample. After annealing experiment, the water concentration was also measured and calibrated from Paterson (1982) with integration range chosen to be 2,000–4,000 cm^{-1}:

$$C_{OH} = \frac{B}{150\xi}\int \frac{H(\upsilon)}{3780-\upsilon}d\upsilon \tag{1}$$

where C_{OH} is the concentration of incorporated water, $H(\upsilon)$ is the absorption coefficient, υ is the wavenumber, and ξ is an orientation factor (fixed to one third in the present study). Density factor, B, is equal to 2,526 and 2,278 wt. ppm H_2O for Fe-free and Fe-bearing ringwoodite, respectively.

2.4. Diffusion Profile Analysis

After diffusion experiment, recovered sample was fixed in epoxy and ground perpendicular to the diffusion interface until the middle part of the sample was reached. Then the section was polished by diamond paste. Grain size (d) measurements were performed on the digitized FE-secondary electron microscope images of the polished section using the intercept method (Mendelson, 1969). Electron probe microanalyzer was used to obtain element maps and diffusion profiles of ringwoodite diffusion couple. For each couple, at least two diffusion profiles were obtained across the diffusion interface with a step of 2 μm, whose deviation was confirmed to be within measurement error.

Boltzmann-Matano method (Crank, 1975; Matano, 1933) was used to determine the iron content-dependent interdiffusion coefficient, with a binary system assumed to be in a semi-infinite media when analyzing the diffusion profile. The sigmoidal function below was used to fit the concentration profile:

$$C(x) = A_0\left(1-\frac{1}{(1+\exp(A_1x+A_2))^{A_3}}\right) \tag{2}$$

where fitting parameters are expressed as A_0, A_1, A_2, and A_3, and the Fe or Mg content changing with distance x is expressed as $C(x)$.

The Matano interface will be obtained once the equation below is satisfied:

$$\int_{C_1}^{C_2} x\mathrm{d}C = 0 \tag{3}$$

where C_1 and C_2 are the maximum and minimum concentrations, respectively, over the diffusion profiles. The Matano interface was defined at $x = 0$.

Finally, the concentration-dependent interdiffusion coefficient was obtained using Boltzmann-Matano analysis below:

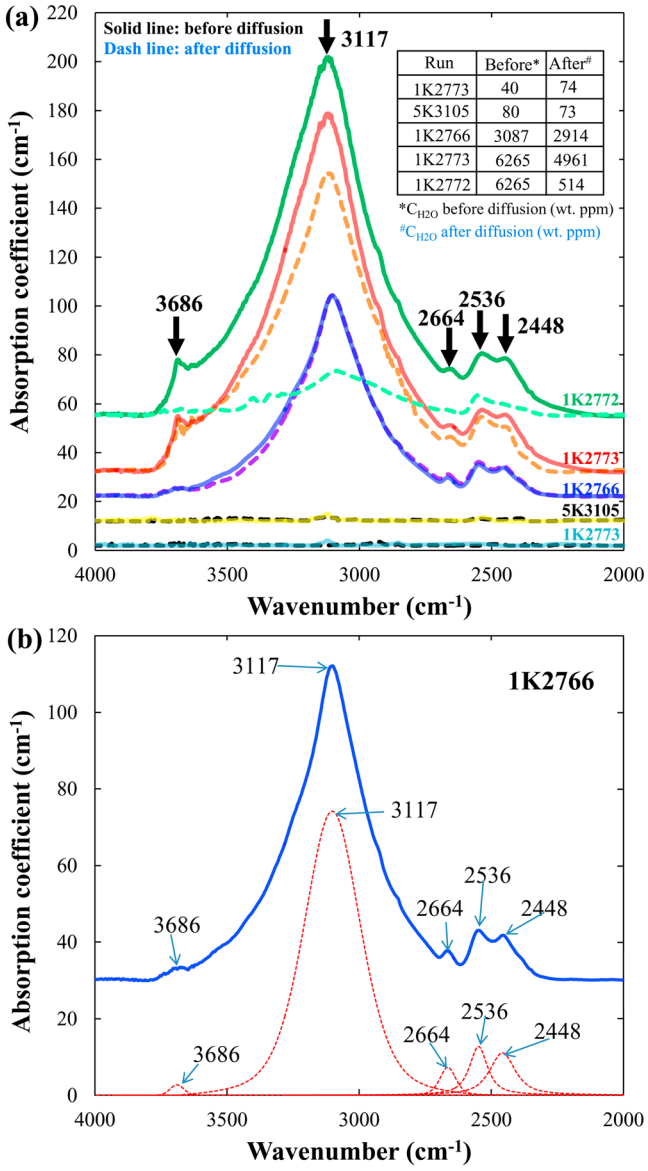

Figure 2. (a) Typical unpolarized Fourier transform infrared spectra for $(Fe_{0.1}Mg_{0.9})_2SiO_4$ ringwoodite part of the diffusion couples before and after diffusion anneals. Note that the absorption spectra for ringwoodite samples with higher water content ~6,000 ppm (runs 1K2772 and 1K2773) show a certain degree of water loss after annealing. (b) Deconvolution of the peaks at 3,686, 3,117, 2,664, 2,536, and 2,448 cm^{-1} for run 1K2766 before diffusion annealing.

$$D(C^*) = -\frac{1}{2t}\left(\frac{dx}{dC}\right)_{C^*}\int_{C_1}^{C^*} x\,dC \quad (4)$$

where experiment duration is denoted as t, and concentration-dependent interdiffusion coefficient is denoted as $D(C^*)$ when concentration is C^*. We can calculate the integral parts by counting squares xdC using equation (4). The gradient $(dx/dC)_{C^*}$ was computed from the tangent of the parabola. The error of diffusion coefficient was estimated from propagated uncertainty from the gradient.

3. Results

Typical unpolarized infrared absorption spectra for Fe-bearing ringwoodite of the diffusion couple before and after diffusion annealing are shown in Figure 2. No significant changes of water content in nominally anhydrous ringwoodite are observed except runs 1K2773 and 1K2772 which show considerable water loss (by 20% and by 90%, respectively; Table 1 and Figure 2a). Hydrous ringwoodite containing 3,000–6,000 wt. ppm H_2O exhibits a main peak at around 3,117 cm^{-1} (Figure 2a). Higher amount of water gives additional peaks at ~3,600 to 3,700 cm^{-1} and ~2,400 to 2,560 cm^{-1}, as also observed in previous studies (e.g., Kohlstedt et al., 1996; Yoshino et al., 2008).

Figure 3a shows the cross section of diffusion couple from run 1K2773 annealed at 20 GPa, 1,373 K for 37 hr under dry condition. The back-scattered electron images show some cracks in ringwoodite aggregates and the bicrystal interface due to thermal shock during quenching. Figure 3b illustrates an element mapping of Fe in the area of Figure 3a (run 1K2773), which demonstrates a diffusion front near parallel with the initial interface. Average grain size in Mg-rich ringwoodite aggregate is generally larger than that of Fe-rich one. The grain sizes of dry ringwoodite aggregates increase slightly after annealing, while those for hydrous ones increase significantly (see Table 1). Higher water content, higher annealing temperature, and longer duration result in larger grain size except for a few runs, suggesting the enhancement of grain growth by water.

Figure 4 shows representative diffusion profiles for run 1K2773 obtained at 20 GPa by electron microprobe (data points) and fitting curves derived from equation (2). In this run, both dry (Figure 4a) and wet (Figure 4b) diffusion couples were simultaneously annealed for 37 hr at 1,373 K. Clearly, hydrous couple shows higher $D_{Fe\text{-}Mg}$ than nominally dry one (Table 1), although it shows partial dehydration (from initial ~6,000 wt. ppm H_2O reduced to ~4,705 wt. ppm H_2O) for run 1K2773. As a result, the diffusion length for hydrous couple (>150 microns in Figure 4b) is longer than that for dry one (~100 microns in Figure 4a). For nominally dry cases, the Matano interfaces are almost the same as their initial interfaces between the two crystals (1K2773, Figure 4a), whereas for hydrous samples, they move slightly to the Mg-rich side relatively to their original interfaces (Figure 4b).

Fe-Mg interdiffusion coefficients for nominally dry and hydrous ringwoodite samples plotted against X_{Fe} is displayed in Figure 5. One obvious feature of the diffusion profiles is the compositional dependence of $D_{Fe\text{-}Mg}$ (Figure 5). As X_{Fe} increases from 0 to 0.1, the diffusivity increases by about 0.5 log unit. Such trend is also observed in Fa-Fo solid solution (e.g., Chakraborty, 1997) and FeO-MgO system (Mackwell et al., 2005; Otsuka & Karato, 2015; Yamazaki & Irifune, 2003). Yamazaki and Irifune (2003) have demonstrated

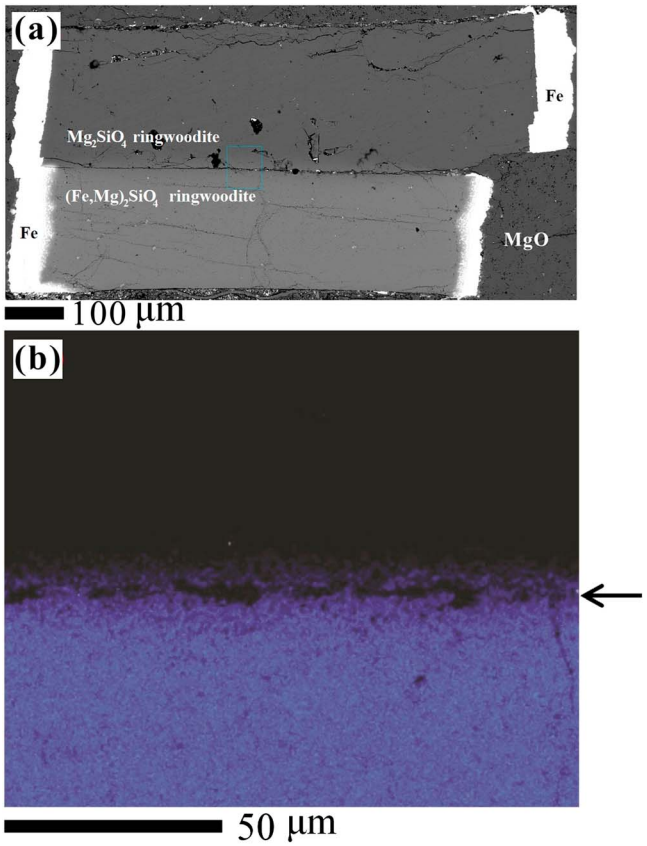

Figure 3. (a) Backscattered electron image of recovered nominally dry diffusion couple (run 1K2773) annealing at 1,373 K, 20 GPa for 37 hr. (b) Element map of iron for the blue dashed rectangle area in (a). The iron content decreases from blue area ($X_{Mg} = 0.9$) at the bottom to black area ($X_{Mg} = 1$) at the top of the image. The black arrow indicates the initial interface.

that Fe-Mg interdiffusivities obtained in intermediate range are more reliable than those determined far from the interface. Therefore, interdiffusivities for $X_{Mg} = 0.94$ and 0.96 are listed in Table 1 for reference.

By considering the strong compositional dependence and large water effect, Fe-Mg interdiffusion coefficients obtained in this study as a function of Fe concentration, water content, and temperature can be fitted by the following equation (Mackwell et al., 2005; Otsuka & Karato, 2015; Yamazaki & Irifune, 2003):

$$D = D_0 X_{Fe}^n C_{H_2O}^r \exp\left[-\left(E^* + \alpha C_{H_2O}\right)/RT\right] \quad (5)$$

where X_{Fe} is the iron concentration, C_{H2O} is the water content in the lattice, $E^* = (1 - X_{Fe})E_{Mg} + X_{Fe}E_{Fe}$ (activation energy for Fe concentration), T is the absolute temperature in K, R is the ideal gas constant, and n, r, and α are constants. As shown in Figure 5, the linear least-squares regression of the global data set to equation (5) yielded $D_0 = 5.59^{+2.90}_{-1.91} \times 10^{-10}$ m^2/s, $n = -0.21 \pm 0.10$, $r = 0.25 \pm 0.03$, $E_{Mg} = 140 \pm 5$ kJ/mol, $E_{Fe} = 4 \pm 2$ kJ/mol, and $\alpha = -24 \pm 4$. We should note that, as mentioned in Figure 2 and Table 1, two hydrous couples with ~6,000 wt. ppm H_2O suffered from considerable water loss during the diffusion annealing. The possible influence could be evaluated if ringwoodite is assumed to have similar hydrogen diffusion rates with forsterite in hydroxylated or dehydroxylated processes (Jollands et al., 2016; Padrón-Navarta et al., 2014). The time required for dehydration and hydrogen reequilibrium for dimensions of our sample is extremely fast, for example, 5 min for 20 μm diameter and 42 min for 100 μm diameter. So the resultant effect of dehydration on diffusivity is negligible, compared with the annealing time of ~20–37 hr for hydrous diffusion couples. Therefore, it is reasonable to adopt the final water content determined from the recovered diffusion couple to make a global fitting of all diffusion data in Figure 5 using equation (5). Figure 6 shows the temperature dependence of $D_{Fe\text{-}Mg}$ at $X_{Mg} = 0.94$ in nominally dry and wet (up to 5,000 wt. ppm H_2O) ringwoodite at 20 GPa. It is obvious that water can significantly enhance $D_{Fe\text{-}Mg}$ in ringwoodite. For example, the rate of Fe-Mg interdiffusion in the water-doped sample (1K2773 with 4,705 wt. ppm) at 1,373 K is around one order of magnitude faster than that of the anhydrous one (Figure 6). This water effect is similar to that of Fe-Mg interdiffusion in garnet recently reported by Zhang et al. (2019).

4. Discussion

4.1. Effect of Grain Size on $D_{Fe\text{-}Mg}$

Diffusion in polycrystalline materials occurs via two mechanisms, volume diffusion and diffusion along grain boundaries. It is well known that grain-boundary diffusion is generally faster than lattice diffusion by many orders (Farber et al., 2000; Fei et al., 2018a, 2018b; Shimojuku et al., 2009). According to the classification and criteria of grain-boundary diffusion (Harrison, 1961; Joesten, 1991; Le Claire, 1963), three kinetic regimes for diffusion denoted as types A, B, and C can be distinguished, which depend upon the magnitude of lattice diffusion coefficients (D_{lat}) and grain boundary diffusion (D_{gb}), as well as the annealing time (t), grain-boundary width (δ), and grain size (d). In type A regime, lattice diffusion length ~$(D_{lat}t)^{1/2}$ is longer than grain size (i.e., $(D_{lat}t)^{1/2} > d/2$) because of long-time annealing, so lattice diffusion is dominant and a near-planar diffusion front can be observed in concentration contours. In type C regime, grain boundary thickness (δ) is much greater than lattice diffusion length ($(D_{lat}t)^{1/2} \ll \delta$) due to very short-time duration (only several hours or less), where only grain-boundary diffusion contributes to diffusion profile. In type B kinetics, the length of lattice diffusion is close to grain size, which is much larger than the grain boundary thickness ($\delta \ll (D_{lat}t)^{1/2} \leq d/2$), so a trace of atoms can only visit an isolated grain boundary and the adjacent grain edges. In the present experiments, the grain size for nominally dry and hydrous ringwoodite aggregates

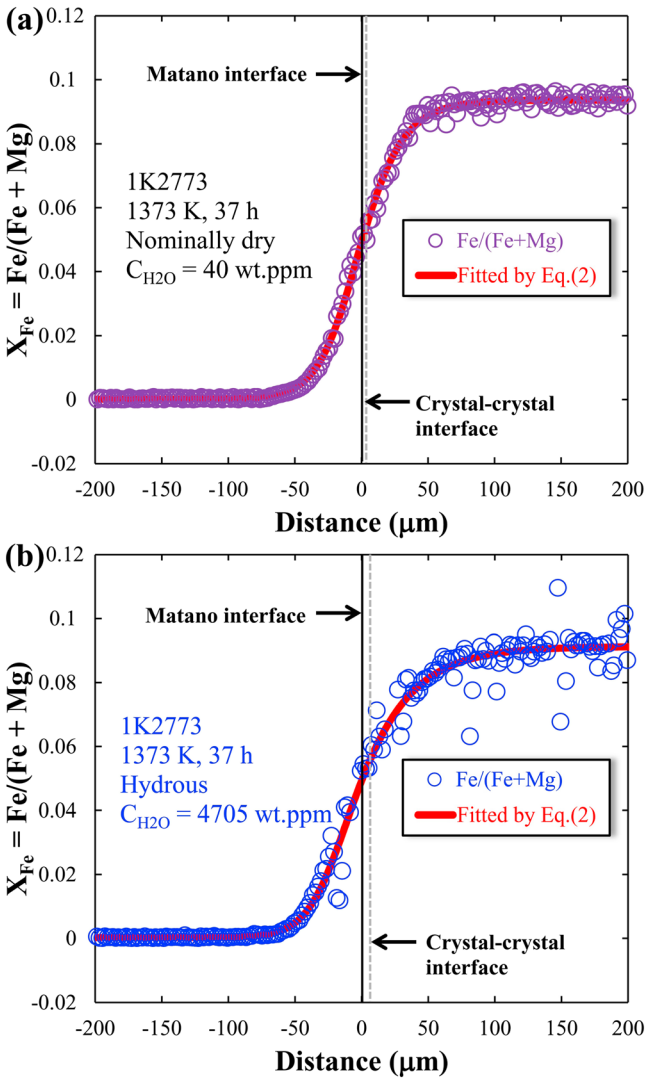

Figure 4. Representative Fe-Mg interdiffusion profiles from the nominally dry (a) and wet samples (b) annealed at 20 GPa and 1,373 K for 37 hr in run 1K2773. The Matano interface is set at $x = 0$. The solid lines show the standard Boltzmann-Matano analysis by equation (2) to the data.

(see Table 1) is comparable to the diffusion distance ($\approx\sqrt{Dt}$= 19–84 μm), which suggests that the diffusion in ringwoodite samples operated in the type-B kinetic regime (Harrison, 1961; Joesten, 1991; Le Claire, 1963).

Next, we consider the contribution of grain boundary diffusion to the effective diffusion of polycrystalline aggregate. Lattice diffusion, together with grain-boundary diffusion, contributes to the measured effective bulk diffusivity of Fe-Mg ($D^{\mathrm{eff}}_{\mathrm{Fe\text{-}Mg}}$),

$$D^{\mathrm{eff}}_{\mathrm{Fe\text{-}Mg}} = D^{\mathrm{lat(bulk)}}_{\mathrm{Fe\text{-}Mg}} + D^{\mathrm{gb(bulk)}}_{\mathrm{Fe\text{-}Mg}} \approx D^{\mathrm{lat}}_{\mathrm{Fe\text{-}Mg}} + \frac{3\delta}{d} D^{\mathrm{gb}}_{\mathrm{Fe\text{-}Mg}} \quad (6)$$

When $D^{\mathrm{lat}}_{\mathrm{Fe\text{-}Mg}} \gg 3\delta D^{\mathrm{gb}}_{\mathrm{Fe\text{-}Mg}}/d$, lattice diffusion dominates bulk diffusivity. In contrast, if $D^{\mathrm{lat}}_{\mathrm{Fe\text{-}Mg}} \ll 3\delta D^{\mathrm{gb}}_{\mathrm{Fe\text{-}Mg}}/d$, grain-boundary diffusion will dominate. So far as we know, there is no reported dependence of $D^{\mathrm{lat}}_{\mathrm{Fe\text{-}Mg}}$ and $D^{\mathrm{gb}}_{\mathrm{Fe\text{-}Mg}}$ on water content and grain size in ringwoodite. Therefore, to know the grain-boundary diffusion contribution to the measured effective bulk diffusivity, indirect evaluation is required. Fei et al. (2018a, 2018b) demonstrated that $D^{\mathrm{lat}}_{\mathrm{Mg}}$ and $\delta D^{\mathrm{gb}}_{\mathrm{Mg}}$ have almost identical pressure, water content, and oxygen fugacity dependence in forsterite, which gave $D^{\mathrm{lat}}_{\mathrm{Mg}} / \delta D^{\mathrm{gb}}_{\mathrm{Mg}}$ a constant value of ~10^5 regardless of variables mentioned above. For various mantle minerals, the grain-boundary width has been estimated to be the same of about 1 nm (Farber et al., 1994; Joesten, 1991). If $D^{\mathrm{lat}}_{\mathrm{Fe\text{-}Mg}} / \delta D^{\mathrm{gb}}_{\mathrm{Fe\text{-}Mg}}$ of ringwoodite is assumed to be of the same order with that of forsterite ($D^{\mathrm{lat}}_{\mathrm{Mg}} / \delta D^{\mathrm{gb}}_{\mathrm{Mg}} \approx 10^5$), the contribution of $D^{\mathrm{gb}}_{\mathrm{Fe\text{-}Mg}}$ to our measured $D^{\mathrm{eff}}_{\mathrm{Fe\text{-}Mg}}$ can be estimated from equation (6).

Figure 7 shows the calculated $D^{\mathrm{gb}}_{\mathrm{Fe\text{-}Mg}}$ at $X_{\mathrm{Mg}} = 0.94$ for nominally anhydrous ringwoodite (~50 wt. ppm H_2O) employing $D^{\mathrm{eff}}_{\mathrm{Fe\text{-}Mg}}$ at $d = 20$ μm. Obviously, $D^{\mathrm{gb}}_{\mathrm{Fe\text{-}Mg}}$ is estimated to be around four orders faster than $D^{\mathrm{lat}}_{\mathrm{Fe\text{-}Mg}}$. At temperature from 1,373 to 1,873 K, $3\delta D^{\mathrm{gb}}_{\mathrm{Fe\text{-}Mg}}/d$ is significantly enhanced with decreasing grain size, which is consistent with the grain size-dependent phenomena in forsterite when $d < 1$ μm (Fei et al., 2018a, 2018b). Furthermore, a comparison of our calculated grain size-dependent $D_{\mathrm{Fe\text{-}Mg}}$ in ringwoodite with that in wadsleyite estimated using data from Kubo et al. (2004) revealed that the effective diffusivity between them is consistent in the whole temperature range investigated (Figure 7). Although both cases have similar water content but different grain sizes, it suggests that the behaviors of Fe-Mg interdiffusion in wadsleyite and ringwoodite are similar.

On the other hand, significant grain growth has taken place during diffusion annealing (Table 1), especially for hydrous diffusion couples. The estimated grain size increments based on our diffusion coefficients and a simple parabolic rate law are roughly consistent with those calculated from the growth kinetics of ringwoodite reported by Yamazaki et al. (2005), suggesting that grain growth here is indeed diffusion-limited process over the timescale of our experiments.

To assess the possible effect of grain growth on diffusion, it is better to carry out time series experiments at various durations with fixed temperature and pressure. Most previous investigations have shown that diffusion coefficients obtained from different annealing durations gave no significant variation, even if there is obvious grain growth, such as Fe-Mg interdiffusion in (Fe,Mg)O (e.g., Demouchy et al., 2007; Yamazaki & Irifune, 2003), olivine, and its high pressure polymorphs (e.g., Chakraborty, 1997; Farber et al., 2000). Although such experiments are unsuccessful in this study, these observations suggest that the Fe-Mg interdiffusion coefficients of ringwoodite here might also not affect significantly grain growth. However, further

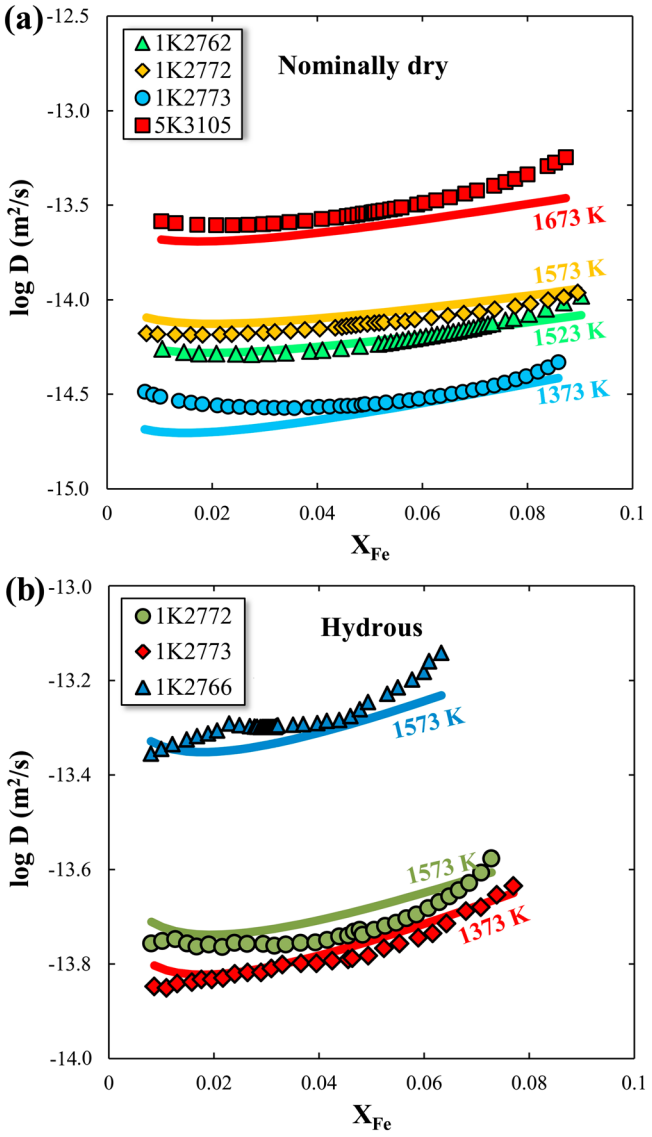

Figure 5. Fe-Mg interdiffusion coefficients in ringwoodite as a function of X_{Fe} at 20 GPa for nominally dry (a) and hydrous (b) diffusion couples using Boltzmann-Matano analyses. The solid lines show the results of the global fit to equation (5) of all the data.

studies are required to determine $D^{lat}_{Fe\text{-}Mg}$ and $D^{gb}_{Fe\text{-}Mg}$ in ringwoodite (and wadsleyite), as well as its grain size and water content dependences.

4.2. Hydrogen Effect on $D_{Fe\text{-}Mg}$ and Diffusion Mechanism

In the present study, our results indicate that at given pressure and temperature, $D_{Fe\text{-}Mg}$ in hydrous ringwoodite without dehydration are appropriately one order of magnitude faster than that measured in anhydrous one (Figure 6), with water exponent $r = 0.25 \pm 0.03$ suggesting a nonnegligible influence of water on $D_{Fe\text{-}Mg}$. For example, the $D_{Fe\text{-}Mg}$ in hydrous ringwoodite at 1,373 K by 5,000 wt. ppm H_2O ($D^{Hydrous}_{Fe\text{-}Mg} = 1.82 \times 10^{-14}$ m^2/s) is significantly larger than that in dry one at the same temperature. It is almost identical to the coefficient at 1,673 K in dry one ($D^{Anhydrous}_{Fe\text{-}Mg} = 2.27 \times 10^{-14}$ m^2/s), corresponding to the effect of 300 K increase of temperature (Figure 6). This observation is similar to that reported in wadsleyite (Kubo et al., 2004) and garnet (Zhang et al., 2019). However, the water exponent for $D_{Fe\text{-}Mg}$ in ringwoodite ($r = 0.25$) is smaller than that in olivine ($r \approx 0.9$, Hier-Majumder et al., 2005) and Mg diffusion in forsterite both within the lattice ($r \approx 1.2$, Fei et al., 2018a) and along the grain boundaries ($r \approx 1.0$, Fei et al., 2018b) and in garnet ($r \approx 1.38$, Zhang et al., 2019).

Although hydrogen entering ringwoodite lattice can significantly enhance diffusion rate, water bonding mechanism and diffusion mechanism remain controversial. Theoretical studies of the defect formation energies from the first principle calculation (Blanchard et al., 2009, 2005; Caracas & Panero, 2017) showed that multiple defect incorporation mechanisms could be identified in ringwoodite, dominated by Mg ↔ 2H (i.e., $[V_{Mg}(OH)_2]^X$) at M site and hydrogarnet defect Si ↔ 4H (i.e., $[V_{Si}(OH)_4]^X$) at T site, and minor amount of Si ↔ Mg + 2H (i.e., $[Mg_{Si}(OH)_2]^X$) (Blanchard et al., 2009, 2005; Caracas & Panero, 2017). Though Purevjav et al. (2014) demonstrated that both tetrahedral and octahedral sites can be simultaneously hydrated in hydrous ringwoodite, infrared spectra of ringwoodite in this study favor the Mg site as hydrogen priority incorporation position. It is seen that the infrared spectra in this study are manifested by a main peak at ~3,110 to 3,130 cm^{-1}, with minor peaks located at ~3,600 to 3,700 cm^{-1} and ~2,400 to 2,560 cm^{-1} (Figure 2a). Following the band assignments based on experimental observations (Kudoh et al., 2000; Mrosko et al., 2013) and first-principle calculations (Blanchard et al., 2009, 2005), the main broadband at around ~3,110 to 3,150 cm^{-1} corresponds to the protonation of octahedral vacancies $[V_{Mg}(OH)_2]^X$, the bands at ~3,500 to 3,700 cm^{-1} may be caused by either silicon vacancies $[V_{Si}(OH)_4]^X$ or Mg replacing Si atoms $[Mg_{Si}(OH)_2]^X$ related to tetrahedral site, while the weak but stable doublet observed at ~2,500 cm^{-1} is attributed to the overtones of vibrations from Si-O bonding rather than OH-stretching bands. Therefore, the most favorable hydrogen position in ringwoodite structure could be related with Mg site here.

A recent experimental study demonstrated that the mobility of hydroxyl defects related to a vacant Mg-octahedron at the M site in ringwoodite is higher than that related to a vacant Si-tetrahedron at the T site (Mrosko et al., 2013). Furthermore, molecular dynamics simulations also showed that the greatest H diffusion rate was yielded by Mg ↔ 2H, followed by Si ↔ Mg + 2H, and slowest rate by hydrogarnet defect Si↔4H (Caracas & Panero, 2017). Thus, one would expect $[(2H)^X_{Me}]$ to be the main diffusing species during diffusion process. Because the product of faction of vacancies X_V and their diffusivity (or mobility) is

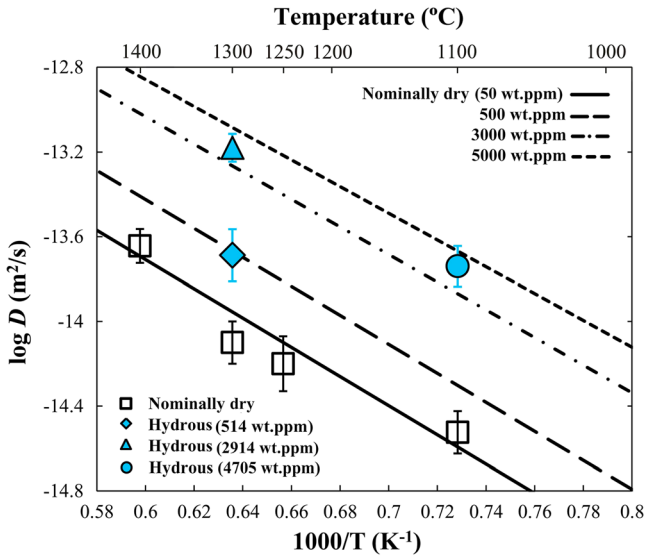

Figure 6. Arrhenius plot of the variation of $D_{Fe\text{-}Mg}$ for $X_{Mg} = 0.94$ in the nominally dry and wet ringwoodite diffusion couples displayed as a function of inverse temperature at 20 GPa. Solid and dashed lines represent the best fit to equation (5) for dry and hydrous cases.

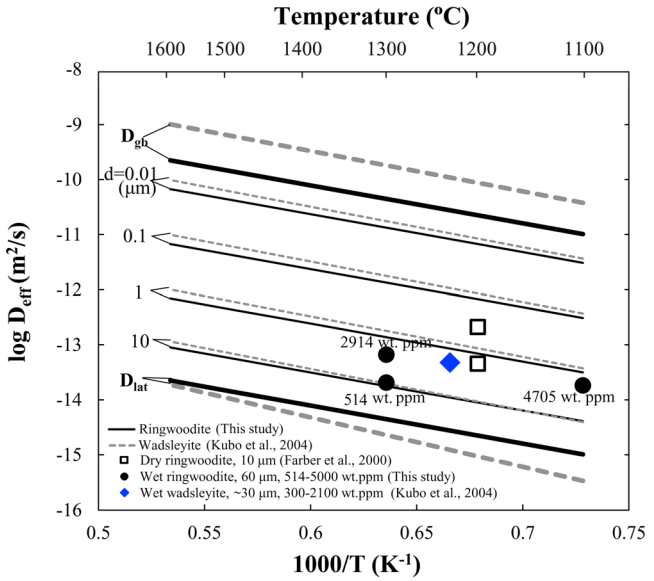

Figure 7. Grain-size dependence of $D_{Fe\text{-}Mg}$ in ringwoodite at 20 GPa and $X_{Mg} = 0.94$ calculated from equation (6) using the diffusion rates with different grain size obtained from the nominally dry diffusion couple (~50 wt. ppm H_2O, solid lines). As a comparison, grain-size dependence of $D_{Fe\text{-}Mg}$ in wadsleyite ($X_{Mg} = 0.90$, 50-90 wt. ppm H_2O and d ~6 μm) at 16-17 GPa using model 1 (Kubo et al., 2004) is also shown in dashed lines. The data from the wet diffusion couples (this study) and previous results (~10 μm; Farber et al., 2000) are shown by solid circles and open squares, respectively. Diamond represents $D_{Fe\text{-}Mg}$ in wadsleyite with 300–2,100 wt. ppm H_2O (Kubo et al., 2004).

proportional to diffusion coefficient D of corresponding cation, we have $D_{Fe\text{-}Mg} \propto X_{V''_{Me}} \times D_{V''_{Me}}$. In present study, we obtain $D_{Fe\text{-}Mg} \propto C_{H_2O}^{0.25}$, suggesting that Fe-Mg interdiffusion in ringwoodite is charge balanced by $[Fe^{\bullet}_{Me}] = [H'_{Me}]$ (Demouchy et al., 2007; Fei & Katsura, 2016; Kohlstedt, 2006). The smaller water content exponent obtained here ($r \approx 0.25 < 1$) also implies that not all hydrogen is involved in diffusion process.

Oxygen fugacity is expected to influence diffusion property by varying the defect concentrations through changing of oxidation state of multivalent element (such as iron) and the resultant defect sites in the structure (e.g., Chakraborty et al., 1994; Dohmen et al., 2007; Mackwell et al., 2005; Otsuka & Karato, 2015; Zhang, 2017). In the present experiments, two different kinds of buffers consisting of Fe capsule (~IW buffer) and Pt capsule (~ΔIW + 2, based on results from Faul et al., 2018) were used for nominally anhydrous and hydrous diffusion couple, respectively. Under anhydrous conditions, the major point defects in $(Mg,Fe)_2SiO_4$ ringwoodite are V''_{Me} and $Fe^{\bullet}_{Me}$ so that the charge neutrality condition is maintained by $[Fe^{\bullet}_{Me}] = 2[V''_{Me}]$, suggesting that $D_{Fe\text{-}Mg} \propto [Fe^{\bullet}_{Me}] = 2[V''_{Me}] \propto fO_2^{1/6}$ (Demouchy et al., 2007; Kohlstedt, 2006; Kohlstedt & Mackwell, 1998).

Under hydrous conditions, hydrogen is incorporated into ringwoodite crystal structure as either positively or negatively charged point defects, that is, $H^{\bullet}_i = (OH)^{\bullet}_O$ or $H'_{Me} = \{(OH)^{\bullet}_O - V''_{Me}\}'$. Due to relatively high fO_2 within Pt capsule in this study, ferric iron would also present in Fe-bearing ringwoodite. Therefore, possible charge neutrality conditions would include (Demouchy et al., 2007; Fei & Katsura, 2016; Kohlstedt, 2006; Kohlstedt & Mackwell, 1998): (i) $[H^{\bullet}_i] = 2[V''_{Me}]$, (ii) $[Fe^{\bullet}_{Me}] = [H'_{Me}]$, and (iii) $[H^{\bullet}_i] = [H'_{Me}]$. Previous studies demonstrated that the charge neutrality condition may change with hydrogen and/or iron concentrations, as well the thermodynamic conditions (Demouchy et al., 2007; Fei & Katsura, 2016; Kohlstedt, 2006). Therefore, at relatively oxidizing condition, the charge neutrality condition in hydrous $(Mg,Fe)_2SiO_4$ ringwoodite here is expected to change from $[Fe^{\bullet}_{Me}] = 2[V''_{Me}]$ to $[Fe^{\bullet}_{Me}] = [H'_{Me}]$ and then $[H^{\bullet}_i] = [H'_{Me}]$ with increasing C_{H2O}. Water content exponent $r = 0.25$ here gives $D_{Fe\text{-}Mg} \propto [Fe^{\bullet}_{Me}] = [H'_{Me}] \propto fH_2O^{1/4} fO_2^{1/8}$, which means that the influence of oxygen fugacity becomes smaller compared with that under dry conditions.

Besides the effects of water and fO_2, variation of silica activity (a_{SiO2}) is also expected to influence the defect concentration and resultant diffusivity (Stocker & Smyth, 1978). In the near-stoichiometric region, the concentrations of the Si defects, for example, Si vacancy ($[V''''_{Si}]$) and interstitial position ($[Si^{\bullet\bullet\bullet\bullet}_I]$), are very sensitive to a_{SiO2}. In contrast, if the charge neutrality condition is maintained by $[Fe^{\bullet}_{Me}] = [H'_{Me}]$ under relatively oxidizing conditions, the concentration of the major point defects (i.e., $[Fe^{\bullet}_{Me}]$, $[H'_{Me}]$, and $[V''_{Me}]$) would be almost independent on a_{SiO2} (Stocker & Smyth, 1978). In fact, Chakraborty et al. (1994) did not report resolvable influence of a_{SiO2} on Mg tracer diffusion rates in olivine. Therefore, it is reasonable to speculate that the effect of a_{SiO2} on $D_{Fe\text{-}Mg}$ is limited in the present experiments. However, more laboratory and theoretical works are required to identify and quantify the detailed effects of fO_2 and a_{SiO2} on the diffusivity in ringwoodite in future.

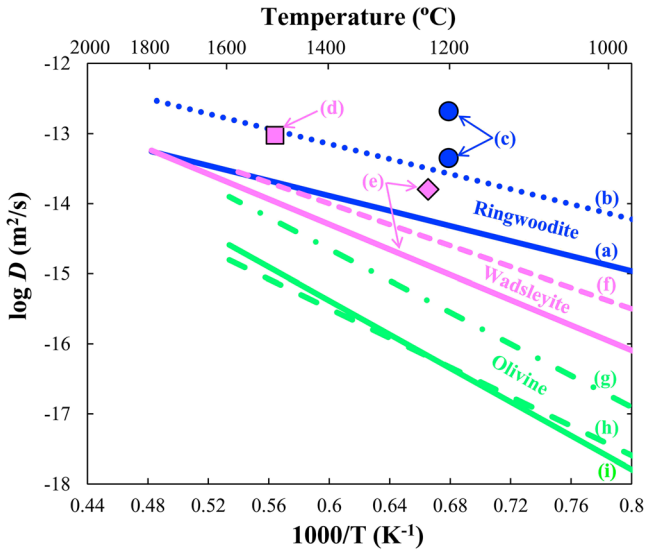

Figure 8. Comparison of Fe-Mg interdiffusion results with data for other mantle minerals. Data for ringwoodite: (a) and (b) represent dry (d = 20 μm, ~50 wt. ppm H_2O) and wet (60 μm, ~3,000 wt. ppm H_2O) cases reported in this study and (c) sample with 10-μm grain size but no water content reported by Farber et al. (2000). Wadsleyite normalized to 16 GPa: (d) from Holzapfel et al. (2009; d = 25–60 μm, 35 wt. ppm H_2O), (e) from Kubo et al. (2004; d = 20 μm, 50–90 wt. ppm H_2O) and the diamond point is also from Kubo et al. (2004) for hydrous wadsleyite (d = 21–37 μm, 300–2,100 wt. ppm H_2O), and (f) from Chakraborty et al. (1999; d = 60–220 μm). Olivine: (g) from Hier-Majumder et al. (2005), (h) from Dohmen et al. (2007), and (i) from Chakraborty (1997).

4.3. Comparison With Previous Studies

Until now, only Farber et al. (2000) reported Mg-Fe interdiffusion coefficient in γ phase under 10–14 GPa and 1,473 K. Their obtained $D_{Fe\text{-}Mg}$ in ringwoodite, if normalized to 20 GPa, is at least one order higher than those determined under anhydrous conditions in this study (Figure 8). This difference possibly arises from either the existence of small amount of water in their samples or higher fO_2 (~Ni-NiO (NNO)) which could lead to increased diffusivity. Another possibility is that their smaller grain size (d = 10 μm) compared with our case (d ~ 20 μm) introduces more contribution from grain-boundary diffusion to the effective diffusivity (Figure 7). Similar phenomena can be observed if previous data of wadsleyite (e.g., Chakraborty et al., 1999; Holzapfel et al., 2009; Kubo et al., 2004) were extrapolated to 16 GPa at NNO buffered condition with 6.1 cm^3/mol adopted as activation volume (Farber et al., 2000). As shown in Figure 8, $D_{Fe\text{-}Mg}$ in wadsleyite with smaller grain size (20 μm, Holzapfel et al., 2009) is much faster than those with larger grain size (60–220 μm, Chakraborty et al., 1999).

Although some previous work did not report the exact water concentration in their experiments (e.g., Chakraborty et al., 1999; Farber et al., 2000; Hier-Majumder et al., 2005), structural water greatly increases $D_{Fe\text{-}Mg}$ in ringwoodite (this study), wadsleyite (Kubo et al., 2004), and olivine (Hier-Majumder et al., 2005). Our study revealed that $D_{Fe\text{-}Mg}$ of ringwoodite is similar with that of wadsleyite, which compared with olivine is one to two log units higher (e.g., Chakraborty, 1997; Dohmen et al., 2007; Hier-Majumder et al., 2005; Figure 8). The nearly identical diffusion rates obtained from wadsleyite and ringwoodite might reflect the structural similarity though their activation energies differ. Unfortunately, quantitative relationship between water content and $D_{Fe\text{-}Mg}$ in wadsleyite and olivine has not yet been established, therefore it remains unknown whether wadsleyite and olivine have similar diffusion rates as that of ringwoodite under the same water concentration.

4.4. Implications for Chemical Heterogeneity in the MTZ

Since cation diffusivities in ringwoodite can be largely enhanced by dissolved water, many geodynamic processes including homogenizing of chemical heterogeneity in the MTZ might be affected by the transport properties of ringwoodite. Considering a simple model for mixing of chemical heterogeneities by combined diffusion and convective flow (Kellogg & Turcotte, 1990), the present data can be applied to evaluate time required for equilibration and the length scale of heterogeneities in the MTZ produced by convective stirring.

It is well-known that the thickness of subducted oceanic crust would be reduced following the exponential form $h = h_0 \exp\left(-\dot{\varepsilon}t\right)$ by stirring in the mantle (Kellogg & Turcotte, 1990), where $\dot{\varepsilon}$ is the strain rate, h_0 is the subducted oceanic crust thickness at beginning, and h is its thickness after duration of t. When typical strain rates of ~3×10^{-16} to 3×10^{-15} s^{-1} were used (Holzapfel et al., 2005), an initial thickness (~7 km) of the oceanic crust is reduced to the diffusion length scale in approximately 0.1–1 Ga (Figure 9). In addition, the rate of chemical diffusion could affect the preservation of subducting oceanic slab. The diffusion rate can be used to confine the characteristic length scale x using the equation $x = 2\sqrt{D_{\text{eff}}t}$, where D_{eff} is the effective diffusion coefficient. Because the MTZ contains significant amount of majoritic garnet, a parallel mixing model assuming 60 vol.% ringwoodite plus 40 vol.% majoritic garnet was adopted. In this calculation, experimental results of $D_{Fe\text{-}Mg}$ for ringwoodite (this study) and garnet measured under dry and wet conditions were also considered (Zhang et al., 2019), which corresponds to the lower and upper bounds of the characteristic distance. Due to the opposing effects between pressure (activation volume of 2.04 cm^3/mol due to Mg vacancy diffusion reported by Verma & Karki, 2009) and temperature on diffusion along the mantle geotherm (Katsura et al., 2010), $D_{Fe\text{-}Mg}$ are almost constant in the MTZ with ~2×10^{-14} and 2×10^{-13} m^2/s for dry and hydrous ringwoodite and ~1×10^{-18} and 3×10^{-16} m^2/s for dry and hydrous majoritic garnet.

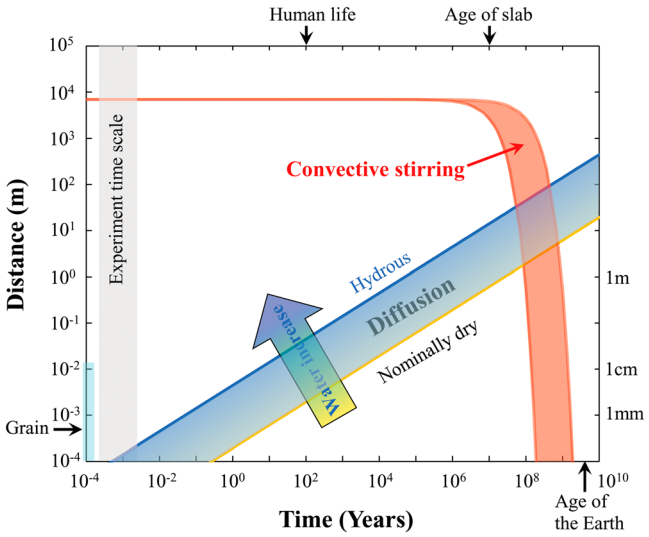

Figure 9. Evolution of length scales relevant to the survival of heterogeneity in the mantle. (Red) Flow-induced thinning of heterogeneity with initial thickness equal to that of present day oceanic crust (7 km) assuming exponential thinning (see text) and values of the strain rate ranging from 3×10^{-16} to 3×10^{-15} s^{-1} estimated from an average convection velocity of 5 cm/year (Holzapfel et al., 2005). Yellow and Blue lines represent the nominally dry and wet cases for a mixing model (see text) in the mantle transition zone. The heterogeneity is assumed to have the form of a sphere. In this calculation, chemical homogenization is assumed to be achieved when the elemental concentration has fallen to 5% of its original value.

Figure 9 shows the cation diffusion length after 100 Ma which is only ~50 m for hydrous case and ~10 m for anhydrous case. Even assuming the entire Earth age (4.5×10^9 years), the scale of heterogeneities in the MTZ equilibrated by volume diffusion ranges from ~50 to 400 m depending on water content. If lattice diffusion dominates the material mixing process, the re-equilibrated size would be less than 100 m within one cycle of convection (roughly equal to the timescale of the subducted slab age ~50 to 200 Ma) in the MTZ. In both cases, the equilibrated range is tiny (<100 m) when compared with thickness of subducting slab and MTZ. Despite water can greatly enhance cation diffusion rates in major mantle minerals in the MTZ, very limited length scales (<500 m) for the homogenization of chemical heterogeneities is calculated by $D_{Fe\text{-}Mg}$ data, even when the timescale of Earth age was assumed. It suggests the ineffectiveness in hydration of nearby mantle and long-term preservation of chemical heterogeneity of subducted slabs.

Besides the effect of water on $D_{Fe\text{-}Mg}$, as illustrated in Figures 6–8, the effective diffusivity also depends on grain size because grain-boundary diffusion could be greatly enhanced by decreasing grain size. Although the real grain size in the MTZ has remained enigmatic for decades, Riedel and Karato (1997) have indicated that the response of grain size in subducted oceanic lithosphere accompanying phase transition of olivine to spinel is very sensitive to temperature and pressure. As a result, variation of grain size derived from experimental observation is from several tens micrometers to millimeters in the P-T conditions of the MTZ, whereas grain size derived from theoretical calculations is ~10^3–10^7 m (Riedel & Karato, 1997). Obviously, actual grain size in the MTZ is much larger (or at least equivalent) than that used in the present estimation for chemical heterogeneity, which suggests that the chemical homogeneity estimated here provide an upper limit and any increase of grain size would result in even smaller scale of chemical reequilibrium since effective diffusivity would be reduced with larger grain size. Therefore, the conclusion in Figure 9 holds.

4.5. Implications on the Electrical Property of the MTZ

In this part, the cation contribution to electrical conductivity in ringwoodite was calculated, and the possible water storage in the MTZ was estimated. Under anhydrous conditions, electrical conductivity measurements on Fe-bearing mantle silicates indicate that the primary charge carriers are M site related vacancies (i.e., $[V_{Mg}'']$), as well as polarons and electrons (Yoshino, 2010). However, when water is present, hydrogen-induced point defects (i.e., free proton $H^{\bullet}$) could be alternative charge carriers. Thus, the bulk conductivity of hydrous ringwoodite (σ_{Bulk}) could be estimated by adding the dry ringwoodite conductivity (σ_{Dry}, sum of hopping conduction and ionic conduction) with the contribution from hydrogen (σ_{Wet}):

$$\sigma_{Bulk} = \sigma_{Dry} + \sigma_{Wet} \tag{7}$$

In this study, hopping conduction of anhydrous ringwoodite aggregates reported by Yoshino et al. (2008) was adopted. Combined cation diffusivity in ringwoodite (Sun et al., 2015) with our data under anhydrous and hydrous conditions, the diffusion of charged species i resultant ionic- or water-related conductivity σ_i is related to the corresponding concentration and diffusivity, through the Nernst-Einstein equation:

$$\sigma_i = \frac{D_i (z_i F)^2 c_i}{RT} \tag{8}$$

where z_i is the charge of the migrating species, F is Faraday's constant, T is the temperature, and R is the gas constant.

By combination of equations (7) and (8), hydrogen-related vacancy and bulk conductivity calculated for hydrous ringwoodite from Sun et al. (2015) and our present study are consistent with those direct

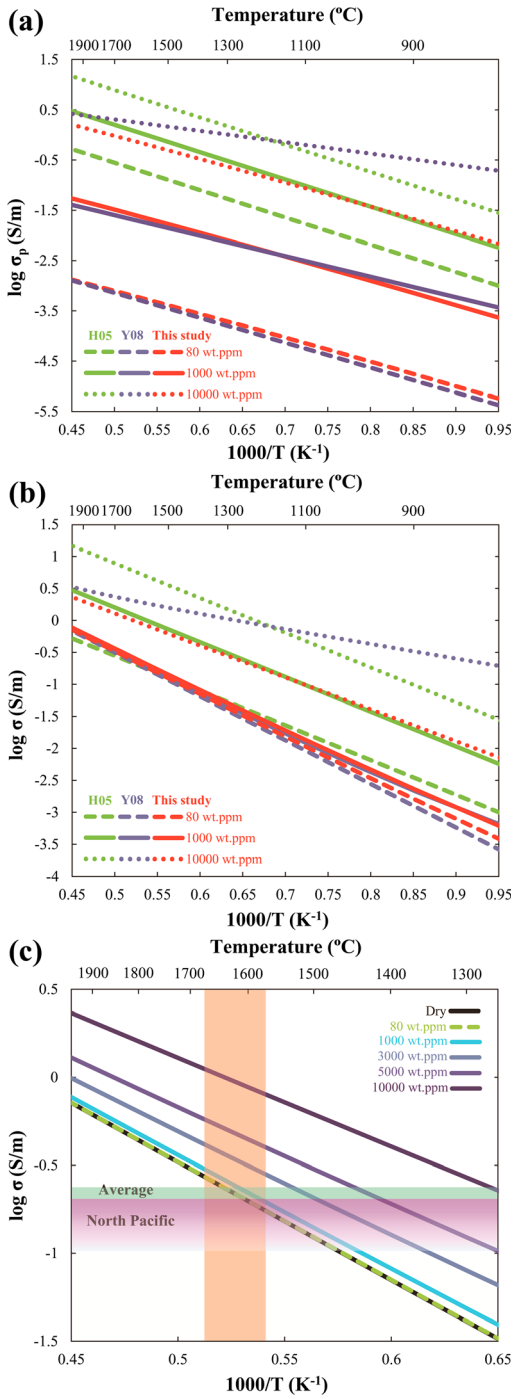

Figure 10. (a) Proton and (b) bulk conductivity in ringwoodite with different water contents (80, 1,000, and 10,000 wt. ppm H_2O displayed by dashed, solid, and dotted lines, respectively) as a function of reciprocal temperature. H05 and Y08 represent olivine data from Huang et al. (2005) and Yoshino et al. (2008) and shown by blue lines, respectively, while red lines denoted the calculated conductivities from this study (including hydrogen self-diffusivity by Sun et al., 2015). Small polaron conduction was applied from the results of dry ringwoodite (Yoshino et al., 2008). (c) Ringwoodite electrical conductivity as a function of inverse temperature and H_2O content. Calculations are shown for dry ringwoodite (Yoshino et al., 2008) as well as hydrous (this study), with 80, 1,000, 3,000, 5,000, and 10,000 wt. ppm H_2O. The light blue and purple regions (horizontal) denote ranges of conductivity values observed in the global average model (Kelbert et al., 2009) and in the North Pacific Ocean (Shimizu et al., 2010), respectively. The adiabatic temperatures calculated at depth of 520–660 km (~1,850–1,950 K; Katsura et al., 2010) are also shown in orange band (vertical). For hydrous conditions, the conductivities due to protons and ions were calculated under the assumption that all of the protons and all of Mg vacancies contributed to electrical conduction, even those tied up in charge-neutral defect associates.

conductivity measured by Yoshino et al. (2008) at relatively low water concentration (<1,000 wt. ppm H_2O) in the temperature range of MTZ (1,600–2,000 K) but ~2 log units smaller than that from Huang et al. (2005; Figure 10a). The hydrogen self-diffusion-induced activation enthalpy of ringwoodite (101 kJ/mol; Sun et al., 2015) is comparable with that determined from water-related conductivity (103–108 kJ/mol; Huang et al., 2005; Yoshino et al., 2008) at low water content. But at higher water content, the calculated results from this study and Sun et al. (2015) are much lower than those measured by Huang et al. (2005) and Yoshino et al. (2008; Figure 10a). Some possible reasons might explain such discrepancy of water-induced conductivities among different laboratories. First, Huang et al. (2005) did not distinguish the contribution of water-related conduction from that of small polaron conduction. Consequently, their conductivity data were dependent on water content as shown in Figure 10a, which means only water-related conduction was considered for hydrous ringwoodite at all temperature range. Second, in the direct laboratory conductivity measurements, water effect on conduction might be overestimated, especially at higher water content due to possible dehydration (Yoshino & Katsura, 2012). Moreover, if the mobility of free proton is much faster than that of $(2H)_M^X$, it would dominate conductivity, resulting in a lower activation enthalpy. Karato (2013) argued that conductivity is dominated by free protons at lower temperatures, while at higher temperatures, it is dominated by more abundant but less mobile defect $(2H)_M^X$. Yoshino et al. (2008) observed a large decrease of ΔH when water content increased, and a term of $\alpha C_{H2O}^{1/3}$ was introduced to fit their conductivity data. However, such phenomena were not found in $D_{Fe\text{-}Mg}$ from this study and D_H from Sun et al. (2015). Reduction of ΔH with increasing water content is not due to single diffusion mechanism. At high temperatures, the activation enthalpy in hydrous ringwoodite from Yoshino et al. (2008) suggested that the amount of highly moving interstitial $H^\bullet$ species increased with water content nonlinearly (Sun et al., 2015) and the grain boundary effect became dominant at high water content.

At higher temperatures relevant to the MTZ, Mg vacancy [V_{Mg}''] and small polaron might become dominant rather than water-related conduction, because the activation enthalpies for ionic and small polaron conduction become greater (Yoshino, 2010). Considering the three conduction mechanisms simultaneously, Figure 10b shows the bulk conductivity of ringwoodite. It is clear when compared with the hopping conduction, the water contribution to ringwoodite bulk conductivity is insignificant.

Figure 10c illustrates the relationship of water content and temperature effect on the MTZ. The average conductivity observed in the North Pacific Ocean (Shimizu et al., 2010) and revealed from Kelbert et al.'s (2009) global average model could be well explained by ~0.1 wt.% water and temperature of ~1,850–1,950 K (Katsura et al., 2010) in the lower MTZ (~$10^{-0.6}$–10^{-1} S/m). This estimation agrees with Yoshino et al.'s (2008) model and recent studies using seismicity from Jacobsen et al. (2004) and Mao et al. (2012), as well as model based on hydrogen diffusion (Sun et al., 2015). The seismic and electromagnetic tomography anomalies from the northwestern Pacific (Fukao et al., 2004) was reevaluated by Koyama et al. (2006), who concluded that ~0.3 wt% H_2O would be enough to explain anomaly in the MTZ above the stagnant slab. Unfortunately, little evidence is provided to show that the stagnant slab in the northwestern Pacific is more hydrous than surrounding MTZ (Fukao et al., 2004). However, an upper limit of Mg vacancies contribution to wet ringwoodite conductivity could be evaluated from experimentally determined cation diffusivity when all of hydrogen and all of octahedral vacancies are assumed to be contributed to electrical conduction. According to experimentally determined water concentration dependence of conductivity (Huang et al., 2005) and diffusivity (Hier-Majumder et al., 2005), it was suggested that a fraction of hydrogen is bonded and the amount of freely moving protons decreases with increasing water content. If so, the actual water content in the MTZ should be higher than current estimation, which would be consistent with seismic (Mao et al., 2012) and electromagnetic observations (e.g., Fukao et al., 2004; Kelbert et al., 2009; Koyama et al., 2006; Shimizu et al., 2010).

In the subduction zone, electromagnetic tomography revealed high conductivity anomalies (~ 1 S/m) beneath Northeastern China (Ichiki et al., 2006) and Philippine Sea (Baba et al., 2010; Koyama et al., 2006) where abnormally high seismic velocities (V_P and V_S are 1.5% and 2% higher than Preliminary reference Earth model, respectively) were observed in stagnant slabs of MTZ (Fukao et al., 2004). Associated with subducted slabs, about ~200–300 K low-temperature anomalies were observed by seismic tomographic study (Fukao et al., 2004). To interpret such high conductivity anomalies, ~1 wt% water in wadsleyite and ringwoodite is required. In addition, the dependence of V_P on H_2O ($\partial V_P/\partial C_{H2O}$) is

estimated to be −0.4 to −0.26 (km/s)/(wt.% H_2O) from sound velocity of hydrous ringwoodite (Jacobsen et al., 2004; Mao et al., 2012). Although hydration of ringwoodite by ~1 wt.% H_2O can lead to the high conductivity profile (Huang et al., 2005; Yoshino et al., 2008) comparable to MT observations, ~1 wt.% water in ringwoodite will largely decrease V_P and V_S (Jacobsen et al., 2004; Mao et al., 2012). This is inconsistent with seismic observation (Fukao et al., 2004; Koyama et al., 2006). Since hydrogen is unable to account for conductivity anomalies, additional or other mechanisms such as chemical composition variations, redox state, partial melt, and supercritical fluid would be needed (e.g., Manthilake et al., 2009; Sun et al., 2015, 2018; Yoshino & Katsura, 2009).

Acknowledgments
As per AGU's Data Policy, the data in this study are listed in the references and supporting information. We thank associate editor Y. Liang, M.C. Jollands, and D.J. Cherniak for their constructive comments that greatly improve the manuscript. Discussion with H.Z. Fei and T. Katsura helped to clarify some issues. We also appreciate the help of Yang Li for characterization of diffusion couples. This study was financially supported by the 1000Plan Program for Young Talents, the Strategic Priority Research Program (B) of Chinese Academy of Sciences (XDB 18010401), National Natural Science Foundation of China (41773056 and 41303048), Science Foundation of Guizhou Province (2017-1196, 2018-1176) to B. Z., and the Ministry of Education, Culture, Sports, Science, and Technology of the Japanese Government, grants 15H05827 and 17H01155 to T.Y. This study was performed using the joint facilities of the Institute for Planetary Materials, Okayama University. The authors declare no competing financial interests.

References

Baba, K., Utada, H., Goto, T. N., Kasaya, T., Shimizu, H., & Tada, N. (2010). Electrical conductivity imaging of the Philippine Sea upper mantle using seafloor magnetotelluric data. *Physics of the Earth and Planetary Interiors*, *183*(1), 44–62.

Blanchard, M., Balan, E., & Wright, K. (2009). Incorporation of water in iron-free ringwoodite: A first-principles study. *American Mineralogist*, *94*(1), 83–89.

Blanchard, M., Wright, K., & Gale, J. D. (2005). A computer simulation study of OH defects in Mg_2SiO_4 and Mg_2GeO_4 spinels. *Physics and Chemistry of Minerals*, *32*(8–9), 585–593.

Caracas, R., & Panero, W. R. (2017). Hydrogen mobility in transition zone silicates. *Progress in Earth and Planetary Science*, *4*(1), 9.

Chakraborty, S. (1997). Rates and mechanisms of Fe-Mg interdiffusion in olivine at 980°–1300°C. *Journal of Geophysical Research*, *102*(B6), 12,317–12,331.

Chakraborty, S. (2008). Diffusion in solid silicates: A tool to track timescales of processes comes of age. *Annual Review of Earth and Planetary Sciences*, *36*, 153–190.

Chakraborty, S., Farver, J. R., Yund, R. A., & Rubie, D. C. (1994). Mg tracer diffusion in synthetic forsterite and San Carlos olivine as a function of P, T and fO_2. *Physics and Chemistry of Minerals*, *21*(8), 489–500.

Chakraborty, S., Knoche, R., Schulze, H., Rubie, D. C., Dobson, D., Ross, N. L., & Angel, R. J. (1999). Enhancement of cation diffusion rates across the 410-kilometer discontinuity in Earth's mantle. *Science*, *283*(5400), 362–365.

Crank, J. (1975). *The mathematics of diffusion* (2nd ed., pp. 1–414). London: Oxford University Press.

Demouchy, S., Mackwell, S. J., & Kohlstedt, D. L. (2007). Influence of hydrogen on Fe–Mg interdiffusion in (Mg,Fe)O and implications for Earth's lower mantle. *Contributions to Mineralogy and Petrology*, *154*(3), 279–289.

Dohmen, R., Becker, H. W., & Chakraborty, S. (2007). Fe–Mg diffusion in olivine I: Experimental determination between 700 and 1200 °C as a function of composition, crystal orientation and oxygen fugacity. *Physics and Chemistry of Minerals*, *34*(6), 389–407.

Farber, D. L., Williams, Q., & Ryerson, F. J. (1994). Diffusion in Mg_2SiO_4 polymorphs and chemical heterogeneity in the mantle transition zone. *Nature*, *371*, 693–695.

Farber, D. L., Williams, Q., & Ryerson, F. J. (2000). Divalent cation diffusion in Mg_2SiO_4 spinel (ringwoodite), β phase (wadsleyite), and olivine: Implications for the electrical conductivity of the mantle. *Journal of Geophysical Research*, *105*(B1), 513–529.

Faul, U. H., Cline, C. J. II, Berry, A., Jackson, I., & Garapić, G. (2018). Constraints on oxygen fugacity within metal capsules. *Physics and Chemistry of Minerals*, *45*(6), 497–509.

Fei, H., Hegoda, C., Yamazaki, D., Wiedenbeck, M., Yurimoto, H., Shcheka, S., & Katsura, T. (2012). High silicon self-diffusion coefficient in dry forsterite. *Earth and Planetary Science Letters*, *345*, 95–103.

Fei, H., & Katsura, T. (2016). Si and O self-diffusion in hydrous forsterite and iron-bearing olivine from the perspective of defect chemistry. *Physics and Chemistry of Minerals*, *43*(2), 119–126.

Fei, H., Koizumi, S., Sakamoto, N., Hashiguchi, M., Yurimoto, H., Marquardt, K., et al. (2018a). Mg lattice diffusion in iron-free olivine and implications to conductivity anomaly in the oceanic asthenosphere. *Earth and Planetary Science Letters*, *484*, 204–212.

Fei, H., Koizumi, S., Sakamoto, N., Hashiguchi, M., Yurimoto, H., Marquardt, K., et al. (2018b). Pressure, temperature, water content, and oxygen fugacity dependence of Mg grain-boundary diffusion coefficient in forsterite. *American Mineralogist*, *103*(9), 1354–1361.

Fukao, Y., Koyama, T., Obayashi, M., & Utada, H. (2004). Trans-Pacific temperature field in the mantle transition region derived from seismic and electromagnetic tomography. *Earth and Planetary Science Letters*, *217*(3), 425–434.

Harrison, L. G. (1961). Influence of dislocations on diffusion kinetics in solids with particular reference to the alkali halides. *Transactions of the Faraday Society*, *57*, 1191–1199.

Hier-Majumder, S., Anderson, I. M., & Kohlstedt, D. L. (2005). Influence of protons on Fe-Mg interdiffusion in olivine. *Journal of Geophysical Research*, *110*, B02202. https://doi.org/10.1029/2004JB003292

Holzapfel, C., Chakraborty, S., Rubie, D. C., & Frost, D. J. (2009). Fe–Mg interdiffusion in wadsleyite: The role of pressure, temperature and composition and the magnitude of jump in diffusion rates at the 410km discontinuity. *Physics of the Earth and Planetary Interiors*, *172*(1), 28–33.

Holzapfel, C., Rubie, D. C., Frost, D. J., & Langenhorst, F. (2005). Fe–Mg interdiffusion in $(Mg,Fe)SiO_3$ perovskite and lower mantle reequilibration. *Science*, *309*(5741), 1707–1710.

Huang, X., Xu, Y., & Karato, S. (2005). Water content of the mantle transition zone from the electrical conductivity of wadsleyite and ringwoodite. *Nature*, *434*, 746–749.

Ichiki, M., Baba, K., Obayashi, M., & Utada, H. (2006). Water content and geotherm in the upper mantle above the stagnant slab: Interpretation of electrical conductivity and seismic P-wave velocity models. *Physics of the Earth and Planetary Interiors*, *155*, 1–15.

Inoue, T., Yurimoto, H., & Kudoh, Y. (1995). Hydrous modified spinel, $Mg_{1.75}SiH_{0.5}O_4$: A new water reservoir in the mantle transition region. *Geophysical Research Letters*, *22*, 117–120.

Irifune, T., Kawakami, K., Arimoto, T., Ohfuji, H., Kunimoto, T., & Shinmei, T. (2016). Pressure-induced nano-crystallization of silicate garnets from glass. *Nature Communications*, *7*, 13753.

Jacobsen, S. D., Smyth, J. R., Spetzler, H., Holl, C. M., & Frost, D. J. (2004). Sound velocities and elastic constants of iron-bearing hydrous ringwoodite. *Physics of the Earth and Planetary Interiors*, *143*, 47–56.

Joesten, R. (1991). Grain-boundary diffusion kinetics in silicate and oxide minerals. In J. Ganguly (Ed.), *Diffusion, atomic ordering, and mass transport: Selected problems in geochemistry* (pp. 345–395). New York: Springer-Verlag.

Jollands, M. C., Padrón-Navarta, J. A., Hermann, J., & O'Neill, H. S. C. (2016). Hydrogen diffusion in Ti-doped forsterite and the preservation of metastable point defects. *American Mineralogist*, *101*, 1560–1570.

Karato, S. I. (2013). Theory of isotope diffusion in a material with multiple species and its implications for hydrogen-enhanced electrical conductivity in olivine. *Physics of the Earth and Planetary Interiors*, *219*, 49–54.

Katsura, T., Yoneda, A., Yamazaki, D., Yoshino, T., & Ito, E. (2010). Adiabatic temperature profile in the mantle. *Physics of the Earth and Planetary Interiors*, *183*, 212–218.

Kelbert, A., Schultz, A., & Egbert, G. (2009). Global electromagnetic induction constraints on transition-zone water content variations. *Nature*, *460*(7258), 1003–1006.

Kellogg, L. H., & Turcotte, D. L. (1990). Mixing and the distribution of heterogeneities in a chaotically convecting mantle. *Journal of Geophysical Research*, *95*(B1), 421–432.

Kohlstedt, D. L. (2006). The role of water in high-temperature rock deformation. *Reviews in Mineralogy and Geochemistry*, *62*, 377–396.

Kohlstedt, D. L., Keppler, H., & Rubie, D. C. (1996). Solubility of water in the α, β and γ phases of $(Mg,Fe)_2SiO_4$. *Contributions to Mineralogy and Petrology*, *123*(4), 345–357.

Kohlstedt, D. L., & Mackwell, S. J. (1998). Diffusion of hydrogen and intrinsic point defects in olivine. *Zeitschrift für Physikalische Chemie*, *207*(1–2), 147–162.

Koyama, T., Shimizu, H., Utada, H., Ichiki, M., Ohtani, E., & Hae, R. (2006). Water content in the mantle transition zone beneath the North Pacific derived from the electrical conductivity anomaly. *Earth's Deep Water Cycle*, 171–179.

Kubo, T., Shimojuko, A., & Ohtani, E. (2004). Fe–Mg interdiffusion rates in wadsleyite and the diffusivity jump at the 410 km discontinuity. *Physics and Chemistry of Minerals*, *31*, 456–464.

Kudoh, Y., Kuribayashi, T., Mizobata, H., & Ohtani, E. (2000). Structure and cation disorder of hydrous ringwoodite, γ-$Mg_{1.89}Si_{0.98}H_{0.30}O_4$. *Physics and Chemistry of Minerals*, *27*(7), 474–479.

Le Claire, A. D. (1963). The analysis of grain boundary diffusion measurements. *British Journal of Applied Physics*, *14*(6), 351–356.

Mackwell, S., Bystricky, M., & Sproni, C. (2005). Fe–Mg interdiffusion in (Mg,Fe)O. *Physics and Chemistry of Minerals*, *32*(5–6), 418–425.

Manthilake, G., Matsuzaki, T., Yoshino, T., Yamashita, S., Ito, E., & Katsura, T. (2009). Electrical conductivity of wadsleyite as a function of temperature and water content. *Physics of the Earth and Planetary Interiors*, *174*(1), 10–18.

Mao, Z., Lin, J. F., Jacobsen, S. D., Duffy, T. S., Chang, Y. Y., Smyth, J. R., Frost, D. J., et al. (2012). Sound velocities of hydrous ringwoodite to 16GPa and 673K. *Earth and Planetary Science Letters*, *331*, 112–119.

Matano, C. (1933). On the relation between the diffusion coefficients and concentrations of solid metals (the nickel-copper system). *Japanese Journal of Physics*, *8*, 109–113.

Mendelson, M. I. (1969). Average grain size in polycrystalline ceramics. *Journal of the American Ceramic Society*, *52*, 443–446.

Mrosko, M., Lenz, S., McCammon, C. A., Taran, M., Wirth, R., & Koch-Müller, M. (2013). Hydrogen incorporation and the oxidation state of iron in ringwoodite: A spectroscopic study. *American Mineralogist*, *98*(4), 629–636.

Ohtani, E., Litasov, K., Hosoya, T., Kubo, T., & Kondo, T. (2004). Water transport into the deep mantle and formation of a hydrous transition zone. *Physics of the Earth and Planetary Interiors*, *143*, 255–269.

Otsuka, K., & Karato, S. I. (2015). The influence of ferric iron and hydrogen on Fe–Mg interdiffusion in ferropericlase (Mg,Fe)O in the lower mantle. *Physics and Chemistry of Minerals*, *42*(4), 261–273.

Padrón-Navarta, J. A., Hermann, J., & O'Neill, H. S. C. (2014). Site-specific hydrogen diffusion rates in forsterite. *Earth and Planetary Science Letters*, *392*, 100–112.

Paterson, M. S. (1982). The determination of hydroxyl by infrared absorption in quartz, silicate glasses and similar materials. *Bulletin de Mineralogie*, *105*, 20–29.

Purevjav, N., Okuchi, T., Tomioka, N., Abe, J., & Harjo, S. (2014). Hydrogen site analysis of hydrous ringwoodite in mantle transition zone by pulsed neutron diffraction. *Geophysical Research Letters*, *41*, 6718–6724. https://doi.org/10.1002/2014GL061448

Riedel, M. R., & Karato, S. I. (1997). Grain-size evolution in subducted oceanic lithosphere associated with the olivine-spinel transformation and its effects on rheology. *Earth and Planetary Science Letters*, *148*(1–2), 27–43.

Shimizu, H., Koyama, T., Baba, H., & Utada, H. (2010). Revised 1-D mantle electrical conductivity structure beneath the north Pacific. *Geophysical Journal International*, *180*, 1030–1048.

Shimojuku, A., Kubo, T., Ohtani, E., Nakamura, T., Okazaki, R., Dohmen, R., & Chakraborty, S. (2009). Si and O diffusion in $(Mg,Fe)_2SiO_4$ wadsleyite and ringwoodite and its implications for the rheology of the mantle transition zone. *Earth and Planetary Science Letters*, *284*(1), 103–112.

Stocker, R., & Smyth, D. (1978). Effect of enstatite activity and oxygen partial pressure on the point-defect chemistry of olivine. *Physics of the Earth and Planetary Interiors*, *16*, 145–156.

Sun, W., Yoshino, T., Sakamoto, N., & Yurimoto, H. (2015). Hydrogen self-diffusivity in single crystal ringwoodite: Implications for water content and distribution in the mantle transition zone. *Geophysical Research Letters*, *42*, 6582–6589. https://doi.org/10.1002/2015GL064486

Sun, W., Yoshino, T., Sakamoto, N., & Yurimoto, H. (2018). Supercritical fluid in the mantle transition zone deduced from H-D interdiffusion of wadsleyite. *Earth and Planetary Science Letters*, *484*, 309–317.

Verma, A. K., & Karki, B. B. (2009). Ab initio investigations of native and protonic point defects in Mg_2SiO_4 polymorphs under high pressure. *Earth and Planetary Science Letters*, *285*(1), 140–149.

Watson, E. B., & Baxter, E. F. (2007). Diffusion in solid-Earth systems. *Earth and Planetary Science Letters*, *253*(3), 307–327.

Yamazaki, D., Inoue, T., Okamoto, M., & Irifune, T. (2005). Grain growth kinetics of ringwoodite and its implication for rheology of the subducting slab. *Earth and Planetary Science Letters*, *236*(3–4), 871–881.

Yamazaki, D., & Irifune, T. (2003). Fe–Mg interdiffusion in magnesiowüstite up to 35 GPa. *Earth and Planetary Science Letters*, *216*, 301–311.

Yoshino, T. (2010). Laboratory electrical conductivity measurement of mantle minerals. *Surveys in Geophysics*, *31*(2), 163–206.

Yoshino, T., & Katsura, T. (2009). Effect of iron content on electrical conductivity of ringwoodite, with implications for electrical structure in the transition zone. *Physics of the Earth and Planetary Interiors*, *174*(1), 3–9.

Yoshino, T., & Katsura, T. (2012). Re-evaluation of electrical conductivity of anhydrous and hydrous wadsleyite. *Earth and Planetary Science Letters*, *337*, 56–67.

Yoshino, T., Manthilake, G., Matsuzaki, T., & Katsura, T. (2008). Dry mantle transition zone inferred from the conductivity of wadsleyite and ringwoodite. *Nature*, *451*(7176), 326–329.
Zhang, B. H. (2017). An overview of Fe–Mg interdiffusion in mantle minerals. *Surveys in Geophysics*, *38*(4), 727–755.
Zhang, B. H., Li, B. W., Zhao, C. C., & Yang, X. Z. (2019). Large effect of water on Fe–Mg interdiffusion in garnet. *Earth and Planetary Science Letters*, *505*, 20–29.

Erratum

In the originally published version of this article, there were errors in Figures 6 and 8. The errors have been corrected, and this may be considered the authoritative version of record.